Modelling of long waves generated by bottom-tilting wave maker

Lu, Heng; Park, Yong Sung; Cho, Yong Sik

Published in:
Coastal Engineering

DOI:
10.1016/j.coastaleng.2017.01.007

Publication date:
2017

Document Version
Peer reviewed version

Modelling of long waves generated by bottom-tilting wave maker

Heng Lu[a], Yong Sung Park[a,*], Yong-Sik Cho[b]

[a] *School of Science and Engineering, University of Dundee, Perth Road, Dundee DD1 4HN, United Kingdom*
[b] *Civil and Environmental Engineering, Hanyang University, 222 Wangsimni-ro, Seoul 04763, Republic of Korea*

Abstract

In order to generate very long waves in laboratory, a bottom-tilting wave maker is designed and used at the University of Dundee. This new type of wave maker can produce waves longer than solitary wavesin terms of the effective wavelength, which provides better long wave model. Nonlinear and dispersive numerical models are built for modelling the wave tank. A shock-capturing finite volume scheme with high-order reconstruction method is used to solve the governing equations. By comparing to the experimental measurements, the numerical models are verified and able to approximate the resulting waves in the wave tank.

Keywords: nonlinear shallow water equation, Boussinesq equation, linear wave theory, WENO, UNO, wave maker

1. Introduction

Over the last few decades, there have been great interests in tsunami behaviour in near shore region and coastal areas. Among these studies (e.g., Hammack, 1973; Synolakis, 1987; Liu et al., 1995; Li and Raichlen, 2002; Craig, 2006), solitary wave has been the most commonly used tsunami wave model theoretically and experimentally. Indeed one of the reasons that solitary waves have been so popular for such a long time was that they are relatively easy to generate in laboratory (Goring, 1978).

*Corresponding author
Email addresses: h.z.lu@dundee.ac.uk (Heng Lu), y.s.park@dundee.ac.uk (Yong Sung Park), ysc59@hanyang.ac.kr (Yong-Sik Cho)

Solitary wave propagates in constant depth with permanent form, whose surface elevation is described as

$$\eta(x,t) = A_s \,\mathrm{sech}^2\left[K_s(x-ct)\right], \quad K_s = \frac{1}{h_0}\sqrt{\frac{3A_s}{4h_0}}, \tag{1}$$

in the horizontal coordinate x and time t, where η, A_s, c and h_0 denote free surface elevation, wave height, phase velocity and static water depth, respectively. However, recent studies such as Madsen et al. (2008) show that wavelength-to-depth ratios of solitary waves are much smaller than that of tsunamis in reality in the respect of the effective wave period T_s and the effective wavelength L_s of solitary waves:

$$T_s = \frac{2\pi}{K_s c}, \quad \text{and} \quad L_s = \frac{2\pi}{K_s}. \tag{2}$$

In other words, the link between its effective wavenumber K_s and wave height A_s is not realistic. In particular, when tsunamis are approaching the beach, nonlinearity increases significantly, leading to skewness of waves, which is already beyond the KdV scale.

Piston-type wave makers are popular and widely used to generate long waves in laboratory, but the disadvantage is that the wavelength of the generated waves is limited by the stroke length L_p as shown in figure 1. Very few studies mention using bottom-wave-generator to simulate tsunami generation or create long waves. The one designed by Hammack (1973) is well known, which was designed for generating solitary waves excited by positive bed motion under the control of a hydraulic servo-system. We note here that waves generated by sudden bottom motion have been studied in the context of impulsive sloshing in a partially-filled tank (e.g., Kit et al., 1987; Liu and Lin, 2008; Tyvand and Miloh, 2012).

In the present study, a bottom-tilting wave maker at the University of Dundee is investigated. The wave maker is able to generate very long waves, considerably longer than the effective wavelength of solitary waves with same amplitude. The bottom-tilting wave maker is designed based on a simple idea that moving the entire bottom can generate waves as long as the tank itself, which should be the longest wave in any given tank. A schematic drawing of concept of the bottom-tilting wave maker is depicted in figure 1. Note that, in comparison with typical piston-type wave maker,

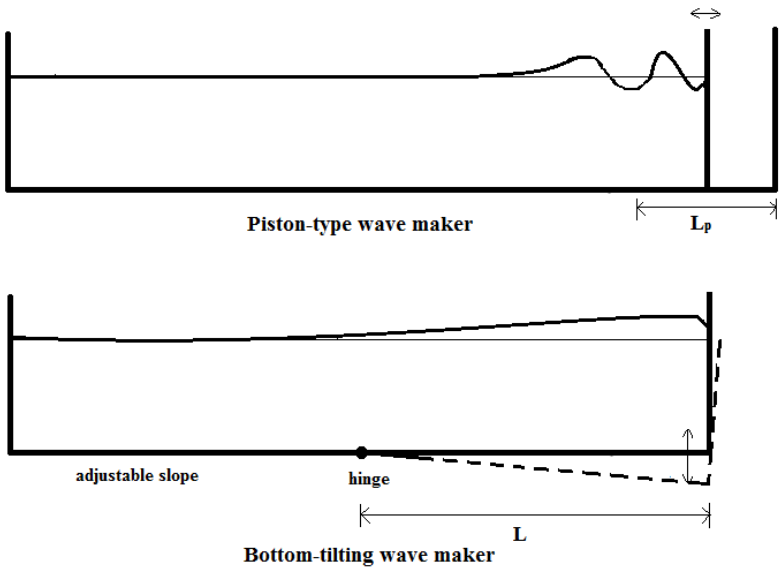

Figure 1: Comparison between piston-type wave maker and the bottom-tilting wave maker.

the bottom tilting wave maker has much longer moving length L, which can produce longer waves. In addition, the generated waves have very short distance to arrive at the shoreline by using the adjustable slope, which can be used to model long wave run-up.

There are a variety of wave theories which have been adopted to examine long waves. In early stage, people evaluated the wave motion from the linear wave theory in tsunami studies. For instance, Kajiura (1963), Keller and Keller (1964), Tuck and Hwang (1972) and Synolakis (1987) have proposed the linear wave theory to approximate near and far field waves. Although, the linear wave theory is limited to situations where nonlinear effects are small for both near and far field waves, it is used as first approximation of long waves in this work.

When nonlinearity makes significant influence, the classical nonlinear shallow water (NSW) equations have been usually employed for simulating waves:

$$\left.\begin{aligned} &\eta_t + ((h+\eta)u)_x + h_t = 0, \\ &u_t + uu_x + g\eta_x = 0, \end{aligned}\right\} \tag{3}$$

where η, u, h and g denote the free surface elevation, the depth-averaged fluid velocity, the static water depth and the gravitational acceleration, respectively. Carrier and Greenspan (1958) proposed an analytical solution to NSW equations for monochromatic waves running up a beach with constant slope. An analytical solution was obtained by Synolakis (1987) for run-up of non-breaking solitary waves. Further development of the analytical solution has been made subsequently, e.g. Antuono and Brocchini (2007), Antuono et al. (2009), Antuono and Brocchini (2010) and Madsen and Schäffer (2010).

On the other hand, frequency dispersion is of great importance during wave generation and propagation when pressure cannot be assumed hydrostatic. Many studies have shown that dispersive models have good performances on long wave simulation (e.g., Peregrine, 1967; Zelt, 1991; Dutykh et al., 2011; Dutykh and Kalisch, 2013). Hence, Boussinesq equations become a good choice to demonstrate the evolution of the surface waves, meanwhile both dispersion and nonlinearity are considered on the basis that they are both small and of the same order of magnitude. Dutykh et al. (2011) introduced a variety of Boussinesq-type wave systems, among which some are applicable for flat bottom and some for arbitrary bottom. In this work, time-dependent bathymetry variations have to be coupled with surface wave. Therefore, the Boussinesq system derived by Wu (1987) for dynamic bathymetry is employed:

$$\left.\begin{aligned} &\eta_t + ((h+\eta)u)_x + h_t = 0, \\ &u_t + g\eta_x + uu_x = \tfrac{1}{2}h(h_t + (hu)_x)_{xt} - \tfrac{1}{6}h^2 u_{xxt}, \end{aligned}\right\} \tag{4}$$

which is an extension of the classical Boussinesq systems.

A wide range of numerical methods are developed in solving these hyperbolic equations, such as finite difference methods, finite element methods, finite volume methods and discontinuous Galerkin methods. Dutykh and Kalisch (2013) used a finite volume scheme to solve the Boussinesq equations for modelling surface waves due to underwater landslides. They demonstrated that finite volume method is good at approximating solutions to conservative equations with high efficiency, accuracy and robustness owing to its conservative and shock-capturing properties. Their numerical results have a good agreement with not only solitary wave propagation and interaction theoretically

but also some experimental measurements. Since how to deal with the discontinuity of discrete solution at the cell interfaces is of key importance, Dutykh et al. (2011) introduced three types of numerical fluxes which can take effect along with some reconstruction techniques such as TVD (Sweby, 1984), UNO (Harten and Osher, 1987) and WENO (Liu et al., 1994) schemes. Among the three types, the central flux, as a Lax-Friedrichs type flux, is chosen in this work. Characteristic flux function is the one Dutykh and Kalisch (2013) used, and confirmed by Dutykh et al. (2011) that it works as well as the central flux. Li and Raichlen (2002) used Lax-Friedrichs flux splitting, which also shows a good performance. For reconstruction techniques, either UNO2 scheme (Harten and Osher, 1987) or WENO scheme uses adaptive stencil to interpolate the numerical flux and keep the piecewise polynomial representations always non-oscillatory. Note that, UNO2 scheme is of second order accuracy while WENO scheme can obtain higher-order accuracy.

The present study introduces the numerical modelling for this new bottom-tilting wave tank system. The fluid is under the assumptions of being inviscid, incompressible and irrotational flow. In addition, bottom dissipation is ignored and full reflection happens at the tank ends. In section 2, linear wave theory is used for preliminary estimation. Then, in section 3 the numerical models considering nonlinearity and dispersion for this specific wave tank are described in detail, including the numerical schemes and methods. By comparing the theoretical and experimental results, this numerical model is validated in section 4. Finally, conclusion remarks are given in section 5.

2. Preliminary estimation by linear wave theory

Figure 2 shows the schematic sketch of the two-dimensional wave tank with a bottom moving in a combined rotating and lifting manner. Clearly, the analysis is divided into two parts at the toe of the slope (hinge). The moving bottom part will generate long waves, and the other part is for the generated waves propagating in the constant water depth or running up the slope. In this section, slope is not considered. The coordinate system origins at the end wall of the generation part, meanwhile the positive x axis is pointing the other end wall and z axis is pointing upwards. Thus, the fluid domain is

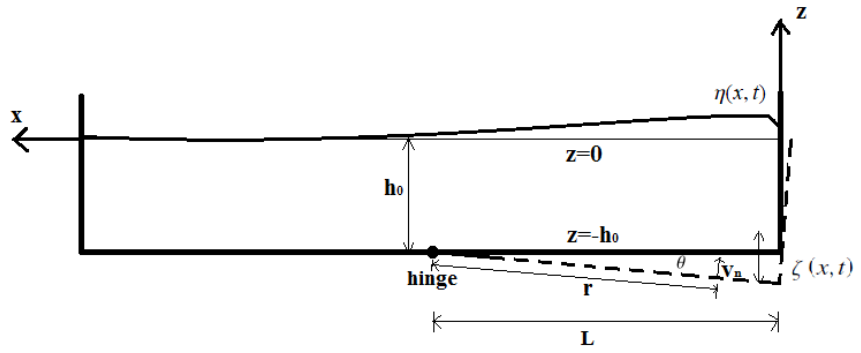

Figure 2: Sketch of the two-dimensional wave maker.

bounded by the two end walls, the free surface and the bottom solid boundary, while the latter two are defined as $z = \eta(x,t)$ on the surface and $z = -h(x,t)$ at the bottom. For $0 < x < L$, water depth is expressed by $h(x,t) = h_0 + \zeta(x,t)$, where ζ denotes the bottom motion displacement, and h_0 the initial water depth.

Linear wave theory is useful for quick estimate of the generated waves, although limited by the conditions that it only applies to non-breaking waves and where non-linear effects are small. The fluid motion in the wave tank can be described by the two-dimensional Laplace equation along with the simplified boundary conditions by linear wave theory. With Φ denoting the velocity potential, continuity equation reads

$$\nabla^2\Phi = \frac{\partial^2\Phi}{\partial x^2} + \frac{\partial^2\Phi}{\partial z^2} = 0, \tag{5}$$

with boundary conditions introduced from the linearised kinematic and dynamic boundary conditions:

$$\frac{\partial\eta}{\partial t} = \frac{\partial\Phi}{\partial z}, \quad z = 0, \tag{6}$$

$$\frac{\partial\Phi}{\partial t} + g\eta = 0, \quad z = 0, \tag{7}$$

$$\frac{\partial\Phi}{\partial z} = 0, \quad z \cong -h_0. \tag{8}$$

Under the assumption that the moving bed is flat, solid and impermeable, the fluid velocity normal to the bed v_n is the same as that of the moving bottom. Thus, the bottom boundary condition becomes

$$v_n = r\frac{\partial \theta}{\partial t}, \tag{9}$$

where r and θ denote rotating radius and angle, respectively. In figure 2, the radius r can be described as $r = (L - x)\sqrt{1 + \tan^2\theta}$ with $0 < x < L$. Since v_n also can be described as

$$v_n = w\cos\theta + u\sin\theta, \tag{10}$$

this leads to

$$(L - x)\sqrt{1 + \tan^2\theta}\frac{\partial \theta}{\partial t} = w\cos\theta + u\sin\theta, \tag{11}$$

where u and w are the horizontal and vertical components of v_n, respectively. For small θ, $w\cos\theta \approx w$, $u\sin\theta \approx 0$, $\tan^2\theta \ll 1$ and $\theta \approx \zeta(x,t)\ (L - x)^{-1}$, hence left-hand side of (11) approximates $\partial\zeta/\partial t$. As a result, the bottom boundary condition (8) becomes

$$\frac{\partial \Phi}{\partial z} = W(x,t) = \frac{\partial \zeta}{\partial t}, \quad z \cong -h_0. \tag{12}$$

In this study, the bottom motion is of finite duration, which can excite the fluid and produce transient waves. Therefore, the Laplace transform in t (denoted by $\bar{}$) and Fourier transform in x (denoted by $\tilde{}$) are applied (Mei, 1989). Then, the equations become

$$\frac{d^2\widetilde{\overline{\Phi}}}{dz^2} - k^2\widetilde{\overline{\Phi}} = 0, \quad -h_0 \le z \le 0, \tag{13}$$

$$\frac{d\widetilde{\overline{\Phi}}}{dz} + \frac{s^2}{g}\widetilde{\overline{\Phi}} = 0, \quad z = 0, \tag{14}$$

$$\frac{\partial\widetilde{\overline{\Phi}}}{\partial z} = \widetilde{\overline{W}}, \quad z = -h_0, \tag{15}$$

where Eq. (14) is obtained by combining Eq. (6) and Eq. (7). Now, the velocity potential is given in the form

$$\Phi(x,z,t) = \frac{1}{2\pi}\int_{-\infty}^{\infty} dk\, e^{ikx}\frac{1}{2\pi i}\int_{\Gamma} ds\, e^{st}\widetilde{\overline{\Phi}}(k,z,s). \tag{16}$$

Under the conditions that $\eta(x,0) = \Phi(x,0) = 0$ and $\overline{\Phi} \to 0$ as $\mid x \mid \to \infty$ within finite t, the solution to the transformed velocity potential is

$$\widetilde{\overline{\Phi}} = \frac{\widetilde{\overline{W}}(s^2 \sinh kz - gk \cosh kz)}{k(s^2+\omega^2)\cosh kh_0}, \tag{17}$$

where $\omega^2 = gk \tanh kh_0$ and k denotes wavenumber. Finally, by substituting Eq. (16) and Eq. (17) into Eq. (6), the solution for the free surface elevation resulting from general bottom motion is obtained as

$$\eta(x,t) = \frac{1}{2\pi}\int_{-\infty}^{\infty} dk \frac{e^{ikx}}{\cosh kh_0} \frac{1}{2\pi i}\int_{\Gamma} ds \frac{s\widetilde{\overline{W}}e^{st}}{s^2+\omega^2}. \tag{18}$$

To apply the solution (18) for the bottom tilting wave maker, we specify the bottom motion displacement as below

$$\zeta(x,t) = D_0(x)\, B(t), \tag{19}$$

where the motion amplitude D_0 is presented as

$$D_0(x) = \begin{cases} a - \frac{a}{L}|x|, & -L \le x \le L, \\ 0, & x < -L \quad \text{and} \quad x > L, \end{cases} \tag{20}$$

with a denoting the motion amplitude at $x = 0$. We note here that the bottom motion amplitude described in (20) is for unbounded domain ($-\infty < x < \infty$) and symmetric with respect to the vertical axis at $x = 0$. Then, (12) becomes

$$\frac{\partial \Phi}{\partial z} = \frac{\partial \zeta}{\partial t} = W(x,t) = D_0(x)\, Q(t), \tag{21}$$

where

$$Q(t) = \frac{dB}{dt}. \tag{22}$$

Taking Fourier transformation of (20),

$$\widetilde{D}_0(k) = \int_{-\infty}^{\infty} D_0(x)\, e^{-ikx} dx = aL \frac{\sin^2(kL/2)}{(kL/2)^2}, \tag{23}$$

in which, we made use of the fact that $D_0(x)$ is an even function. It is straightforward to calculate the solution for impulsive bottom motion, namely, $Q(t) = \delta(t)$. Then, the solution for general bottom motion, $Q(t) = \int_0^t Q(u)\delta(t-u)\, du$, is obtained as a superposition of the impulsive motions:

$$\eta(x,t) = \frac{aL}{\pi}\int_0^t du \int_0^{\infty} dk \, \frac{\sin^2(kL/2)}{(kL/2)^2} \frac{\cos kx}{\cosh kh_0} Q(u) \cos\omega(t-u). \tag{24}$$

3. Numerical model of the bottom-tilting wave maker

Ursell number $U_r = (A/h)\,(kh)^{-2} = \varepsilon\mu^{-2}$ can be used to demonstrate the relation between nonlinearity ε and dispersion μ^2, where $\varepsilon = A/h$ and $\mu = kh$. Thus, the analytical solutions by linear wave theory are useful when $\varepsilon \ll 1$ and $\mu \ll 1$. But in fact, ε is not small in this shallow water tank, so linear wave theory cannot describe the resulting waves accurately. Moreover, dispersion can be important during wave generation and propagation. If both nonlinearity and dispersion are taken into consideration, Boussinesq equations can be a good choice under the condition that the fluid should satisfy $O(\varepsilon) = O(\mu^2) < 1$. However, if $\varepsilon/\mu^2 \gg 1$, in particular during run-up, nonlinear shallow water equations can describe the fluid motion more practically.

After normalisation, the dimensionless variables are given by

$$x^* = \frac{x}{h_0},\ h^* = \frac{h}{h_0},\ \eta^* = \frac{\eta}{h_0},\ t^* = t\sqrt{\frac{g}{h_0}}. \tag{25}$$

For the sake of convenience, asterisk denoting non-dimensionality is dropped in the following discussions.

3.1. Wave generation modelling

Boussinesq equations for time-dependant bathymetry (4) are rewritten in conservative form as below

$$\left.\begin{aligned} &H_t + [Hu]_x = 0, \\ &u_t + [\tfrac{1}{2}u^2 + (H-h)]_x = \tfrac{1}{2}hh_{xtt} + \tfrac{1}{2}h(hu)_{xxt} - \tfrac{1}{6}h^2u_{xxt}, \end{aligned}\right\} \tag{26}$$

where $H = \eta + h$. In order to conform to the conservation law, Eq. (26) are rearranged in the form (Dutykh and Kalisch, 2013):

$$\mathbf{V}_t + [\mathbb{F}(\mathbf{V})]_x = \mathbb{S}_b + \mathbb{M}(\mathbf{V}), \tag{27}$$

where the variable $\mathbf{V}$, the advective flux $\mathbb{F}(\mathbf{V})$, the source term $\mathbb{S}_b$ and the dispersive term $\mathbb{M}(\mathbf{V})$ are denoted respectively by $\mathbf{V} = \begin{pmatrix} H \\ u \end{pmatrix}$, $\mathbb{F}(\mathbf{V}) = \begin{pmatrix} Hu \\ \frac{1}{2}u^2 + (H-h) \end{pmatrix}$, $\mathbb{S}_b = \begin{pmatrix} 0 \\ \frac{1}{2}hh_{xtt} \end{pmatrix}$ and $\mathbb{M}(\mathbf{V}) = \begin{pmatrix} 0 \\ \frac{1}{2}h(hu)_{xxt} - \frac{1}{6}h^2u_{xxt} \end{pmatrix}$.

The finite volume discretization divides a real line $\mathbb{R}$ uniformly into cells $C_i = \left[x_{i-\frac{1}{2}}, x_{i+\frac{1}{2}}\right]$ with centers $x_i = \frac{1}{2}\left(x_{i-\frac{1}{2}} + x_{i+\frac{1}{2}}\right)$ $(i \in \mathbb{Z})$ while Δx_i regarded as the length of the cell. After discretization, the equations become

$$\frac{d\bar{\mathbf{V}}_i}{dt} + \frac{1}{\Delta x}[\mathbb{F}(\mathbf{V}(x_{i+\frac{1}{2}})) - \mathbb{F}(\mathbf{V}(x_{i-\frac{1}{2}}))] = \bar{\mathbb{S}}_i + \bar{\mathbb{M}}_i, \tag{28}$$

where $\bar{\mathbf{V}}_i(t) = \frac{1}{\Delta x}\int_{C_i} \mathbf{V}(x,t)dx$ is regarded as cell average, so as the source term and the dispersive term.

To deal with the discontinuity at cell interfaces in the discrete solution, numerical flux functions are replaced at the cell interfaces by Lax-Friedrichs numerical flux function. For the purpose of achieving higher order approximations to $\mathbf{V}(x_{i\pm\frac{1}{2}}, t)$, a piecewise polynomial representation called UNO2 (Harten and Osher, 1987) is introduced which has a good performance as being of second order accuracy and results in small dissipation in wave computation. On the other hand, WENO type reconstruction can lead to higher order accuracy, for example, 3rd order accurate WENO3 and 5th order accurate WENO5 (Shu, 1998).

For the right-hand side, the second component of the dispersive terms $\mathbb{M}(\mathbf{V})$ are discretized by finite difference scheme:

$$\begin{aligned}
\mathbf{M}_i(\bar{\mathbf{V}}) &= \frac{1}{2}\bar{h}_i\frac{\bar{h}_{i+1}(\bar{u}_t)_{i+1} - 2\bar{h}_i(\bar{u}_t)_i + \bar{h}_{i-1}(\bar{u}_t)_{i-1}}{\Delta x^2} \\
&\quad - \frac{1}{6}\bar{h}_i^2\frac{(\bar{u}_t)_{i+1} - 2(\bar{u}_t)_i + (\bar{u}_t)_{i-1}}{\Delta x^2} \\
&= \frac{\bar{h}_i}{2\Delta x^2}(\bar{h}_{i-1} - \frac{1}{3}\bar{h}_i)(\bar{u}_t)_{i-1} \\
&\quad - \frac{2}{3\Delta x^2}\bar{h}_i^2(\bar{u}_t)_i + \frac{\bar{h}_i}{2\Delta x^2}(\bar{h}_{i+1} - \frac{1}{3}\bar{h}_i)(\bar{u}_t)_{i+1},
\end{aligned} \tag{29}$$

which is of the second order accuracy. The semi-discrete scheme for Boussinesq equations (Dutykh and Kalisch, 2013) can be rewritten as

$$\left.\begin{aligned}
&\tfrac{d\bar{H}}{dt} + \tfrac{1}{\Delta x}\left[\mathbb{F}_+^{(1)}(\bar{\mathbf{V}}) - \mathbb{F}_-^{(1)}(\bar{\mathbf{V}})\right] = 0, \\
&(I - M)\cdot\tfrac{d\bar{u}}{dt} + \tfrac{1}{\Delta x}\left[\mathbb{F}_+^{(2)}(\bar{\mathbf{V}}) - \mathbb{F}_-^{(2)}(\bar{\mathbf{V}})\right] = \mathbb{S}_b^{(2)},
\end{aligned}\right\} \tag{30}$$

where $\mathbb{F}_\pm^{(1,2)}(\bar{\mathbf{V}})$ are the right (+) and left (-) components of the flux vector $\mathbb{F}$, respectively, $\mathbb{S}_b^{(2)}$ is the second component of the source term vector $\mathbb{S}_b$ and M is the diagonal matrix obtained by factoring out $\bar{u}_t$ of the $\mathbf{M}$ as discretized in (29).

Owing to the solid wall on each end, respectively, the boundary conditions are determined as totally reflective. Hence, the horizontal velocity at the wall is imposed to be zero. In addition, ghost cells are added to the boundaries depending on the three different reconstruction methods. According to the finite volume discretization, the imposed boundary conditions are described

$$\begin{cases} H_0 = H_1, \\ (u)_0 = -(u)_1, \\ (u)_{\frac{1}{2}} = 0, \end{cases} \tag{31}$$

where the index 0 indicates the ghost cell.

Time discretization used here is a Runge-Kutta scheme of the third order with four stages proposed by Bogacki and Shampine (1989). The computational domain was discretized with $\delta x = 1/3$, and $\delta t = 0.1$ for computational efficiency and stability. The Courant-Friedrichs-Lewy (CFL) condition, which demonstrates the variants cannot run faster and skip any cell in a single time step, has been verified and satisfied with this discretization. For the equation system (27), the propagation speed is determined by the eigenvalues of the flux Jacobian matrix, where the flux Jacobian matrix is given by

$$\frac{\partial \mathbb{F}(\mathbf{V})}{\partial \mathbf{V}} = \begin{pmatrix} u & H \\ 1 & u \end{pmatrix} \tag{32}$$

and it leads to two eigenvalues defined as

$$\lambda^{\pm} = u \pm c_s, \quad c_s \equiv \sqrt{H}. \tag{33}$$

Therefore, the propagation speed λ cannot exceed the cell speed $\frac{dx}{dt}$, which can be used to define the Courant number as shown below:

$$C_r = \frac{dt}{dx}\max(|\lambda|) \tag{34}$$

and to ensure $C_r < 1$ all the time to satisfy the CFL condition. In fact, by using this discretization, C_r is less than 0.5 at each time step.

In the case where dispersive term $\mathbb{M}(\mathbf{V})$ could be neglected, (27) reduce to NSW equations and are discretized in the form:

$$\frac{d\bar{\mathbf{V}}_\mathbf{i}}{dt} + \frac{1}{\Delta x}[\mathbb{F}(\mathbf{V}(x_{i+\frac{1}{2}})) - \mathbb{F}(\mathbf{V}(x_{i-\frac{1}{2}}))] = \frac{1}{\Delta x}\int_{C_i} \mathbf{S}_b(\mathbf{V})dx \equiv \bar{\mathbb{S}}_i. \tag{35}$$

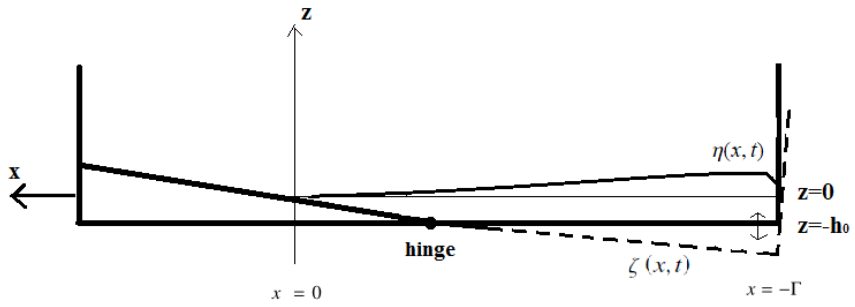

Figure 3: Coordinate system used for run-up modelling

The equations are solved by the same finite volume method for the Boussinesq equation system. Satisfying the CFL condition has been ensured for this scenario as well. Later in section 4.3, this system will be used to compare with the Boussinesq equation system for wave generation. Moreover, nonlinear shallow water equations will also used for wave run-up modelling where nonlinearity plays a key role, which will be discussed in detail in the next section.

It is noted that the WENO5 scheme is used for nonlinear shallow water system as it has higher accuracy. WENO schemes take longer time, but the neglect of the dispersion term saves time for the calculation. For Boussinesq equations, all three reconstruction schemes (UNO2, WENO3 and WENO5) are used and compared to one another, which is further discussed in section 4.1.

3.2. Wave run-up modelling

For sloping beach, the generated wave will soon run up the beach, as shown in figure 3. A corresponding numerical wave model for wave run-up is built based on nonlinear shallow water equations owing to the dominance of nonlinearity during wave run-up. The nonlinear shallow water equations with bottom friction in the conservative

and non-dimensional form are given by

$$\left.\begin{aligned} &H_t + (Hu)_x = 0, \\ &(Hu)_t + (Hu^2 + \tfrac{1}{2}H^2)_x = Hh_x - C_d u|u|, \end{aligned}\right\} \tag{36}$$

because conservative form is beneficial to dealing with the discontinuous solutions. Moreover, for breaking waves, bore is used to model the wave after collapse.

However, because of the difficulties in treating the shoreline position during run-up and run-down on the beach, a computational domain mapping technique (e.g., Zhang, 1996; Li and Raichlen, 2002) is applied to the numerical scheme by transforming the moving space domain into fixed space domain. For convenience, the computation domain is changed, which is now defined as $(-\Gamma, 0)$. $-\Gamma$ is the seaward boundary and 0 is the shoreline where Γ denotes the initial length of the computation domain as shown in figure 3. Hence, the real coordinates are described by the transformed coordinates as below:

$$\left.\begin{aligned} &x = (1 + X/\Gamma)x' + X, \\ &t = t', \end{aligned}\right\} \tag{37}$$

where $X(t)$ is the shoreline position function, x' and t' are the transformed coordinates. Under the transformation, the grid points of the new computation domain will always keep unchanged as the shoreline position $x = X(t)$ always corresponds to $x' = 0$, and the another boundary $x = -\Gamma$ corresponds to $x' = -\Gamma$. In addition, Eq. (37) can lead to the following relations:

$$\left.\begin{aligned} &\frac{\partial}{\partial t} = \frac{\partial}{\partial t'} - \frac{1 + x'/\Gamma}{1 + X/\Gamma} U \frac{\partial}{\partial x'}, \\ &\frac{\partial}{\partial x} = \frac{1}{1 + X/\Gamma} \frac{\partial}{\partial x'}, \end{aligned}\right\} \tag{38}$$

where $U(t) = \frac{dX(t)}{dt}$ indicates the shoreline velocity.

Then, (36) should be modified in the new coordinate system (primes dropped from now on) as below:

$$\left.\begin{aligned} &H_t + (-c_1 UH + c_2 uH)_x = -\tfrac{c_2}{\Gamma} UH, \\ &(Hu)_t + \left(-c_1 UHu + c_2 Hu^2 + \tfrac{1}{2}c_2 H^2\right)_x = c_2 Hh_x - \tfrac{c_2}{\Gamma} UHu - C_d u|u|. \end{aligned}\right\} \tag{39}$$

where $c_1(x, t) = \frac{1+x/\Gamma}{1+X(t)/\Gamma}$ and $c_2(t) = \frac{1}{1+X(t)/\Gamma}$.

Similarly, the equations are rearranged as the form in (35) with the variables $\mathbf{V}$, the advective flux $\mathbb{F}(\mathbf{V})$ and the source term $\mathbb{S}_b$ determined by $\mathbf{V} = \begin{pmatrix} H \\ Hu \end{pmatrix}$, $\mathbb{F}(\mathbf{V}) = \begin{pmatrix} -c_1 UH + c_2 uH \\ -c_1 UHu + c_2 Hu^2 + \frac{1}{2} c_2 H^2 \end{pmatrix}$, and $\mathbb{S}_b = \begin{pmatrix} -\frac{c_2}{\Gamma} UH \\ c_2 H h_x - \frac{c_2}{\Gamma} UHu - C_d u|u| \end{pmatrix}$. In order to solve these equations, the shock-capturing finite volume scheme is still used with the reconstruction of the conservative variables $\mathbf{V}$ by WENO5 scheme and the flux function $\mathbb{F}(\mathbf{V})$ by Lax-Friedrichs central method as well. The same Runge-Kutta scheme is used for time discretization. For modelling the wave tank, computational domain was discretized with $\delta x = 1/3$, and $\delta t = 0.05$, which can ensure the computational efficiency and stability, and satisfy CFL condition.

3.2.1. Boundary condition

Ghost cells are used on the seaward boundary, which is fully reflective. For the shoreward boundary, the boundary elevation and velocity in the transformed computing domain can be defined based on the following relations of Lagrangian descriptions proposed by Zhang (1996):

$$\left.\begin{aligned} & h(X(t)) + \eta(X(t), t) = 0, \\ & \tfrac{dX(t)}{dt} = U(t), \\ & \tfrac{dU}{dt} = -\eta_x. \end{aligned}\right\} \tag{40}$$

Then, according to Beam-Warming scheme and trapezoidal integration, the boundary velocity $U(t)$ and shoreline position $X(t)$ can be estimated by the following schemes of second-order in space and time (Zhang, 1996):

$$\left.\begin{aligned} & U_N^{n+1} = U_N^n - \tfrac{\delta t}{2\delta x}(3\eta_N^n - 4\eta_{N-1}^n + \eta_{N-2}^n) + \tfrac{\delta t^2}{2\delta x^2}(\eta_N^n - 2\eta_{N-1}^n + \eta_{N-2}^n), \\ & X_N^{n+1} = X_N^n + \tfrac{1}{2}\delta t(U_N^{n+1} + U_N^n), \end{aligned}\right\} \tag{41}$$

where N is the last grid index of the transformed computing domain, which indicates the shoreline position all the time. In addition, the two conservative variables on the shoreward boundary are $H(X(t), t) = h(X(t)) + \eta(X(t), t) = 0$ and $Hu(X(t), t) = H(X(t), t) \cdot U(X(t), t) = 0$.

3.2.2. Bottom friction term

Bottom friction terms are commonly used in order to make the numerical results more practical. In this study, a quadratic form $C_d u|u|$ is used in conservative form where C_d is a drag coefficient. C_d also can be defined by $g\,n^2\,H^{-1/3}$ where n denotes the Manning roughness coefficient. It is clearly found from the definition that bottom friction will be very large in shallow water, hence it is not ignorable during run-up since the water depth decreases significantly. The value of C_d can be chosen by comparing some experimental data.

4. Validations and Results

4.1. Wave generation validation

Test of a solitary wave in constant-depth water is used to validate the finite volume scheme for Boussinesq equations by examining if the resulting wave will always keep its shape during its propagation. The solitary wave solution $\eta = A_s\,\mathrm{sech}^2\,[K_s(x - x_0)]$ at $t = 0$ is used as the initial condition, in which x_0 denotes the position of the initial wave crest. Also, $\mathbb{S}_b = \mathbf{0}$ is used for constant depth. Figure 4 displays the solitary waves solved by the finite volume scheme with UNO2, WENO3 and WENO5, respectively. The three numerical methods all closely approximate the exact solution. However, UNO2 reconstruction method is the least time-consuming with comparable accuracy to the other higher-order schemes. Comparably, WENO5 has the highest accuracy. Figure 5 shows the time history of the conservation of mass and energy denoted by V_s and E respectively with the following normalization:

$$V_s^* = \frac{V_s}{h_0^2}, \quad E^* = \frac{E}{\rho g h_0^3}. \tag{42}$$

It is clearly seen that the mass and energy are conserved during the computation for the three reconstruction methods. To maintain consistency in terms of accuracy and well-balanced, only UNO2 scheme is chosen to be used with the second order accurate scheme of the dispersive terms for solving Boussinesq equations, while WENO scheme is used for solving nonlinear shallow water system as no dispersive terms considered.

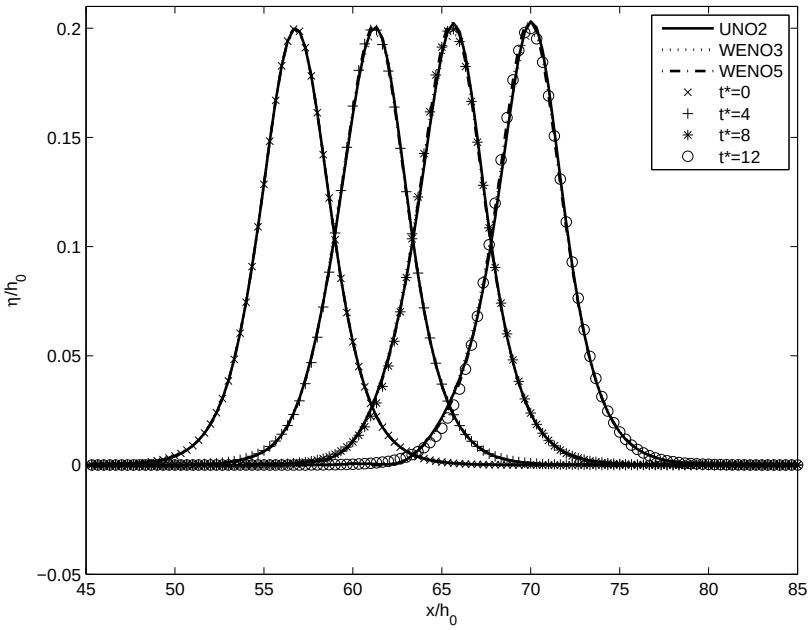

Figure 4: Comparisons of solitary wave among the three schemes (distinguished by line style) and the exact solution (markers) to the solitary wave with $A/h_0 = 0.2$.

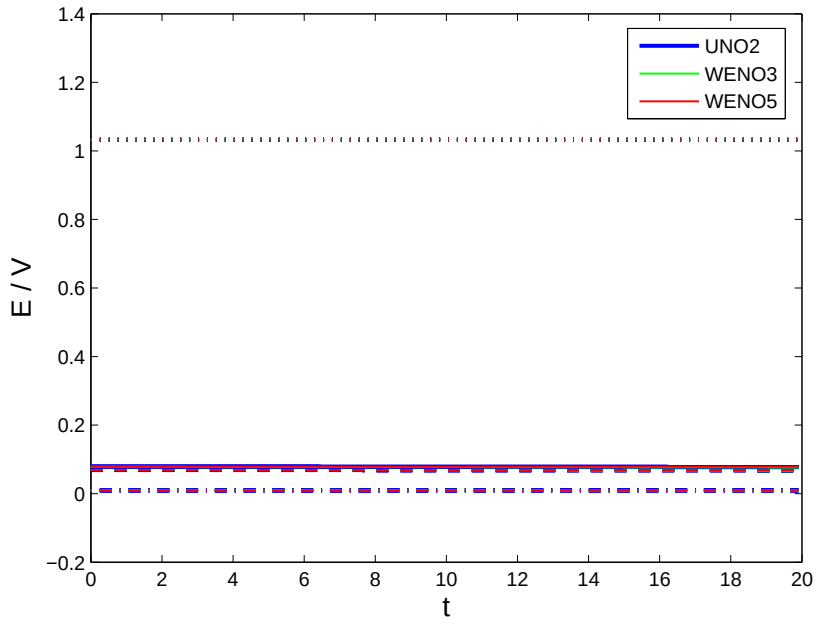

Figure 5: Comparisons of the conservation of mass and energy between the three schemes (dashed line, dash-dot, solid line and dotted line indicate potential energy, kinetic energy, total energy and volume, respectively, while the three schemes are distinguished by colour as marked).

4.2. Wave run-up test cases

The numerical scheme with WENO5 is used to solve nonlinear shallow water system and estimate wave run-up. The method is verified here by producing a time-periodic wave on a sloping beach with amplitude $0 < A \leq 1$ and comparing to the corresponding Carrier-Greenspan periodic solution. Note that bottom friction is neglected here. When amplitude $A = 1$ and $t_0 = 3\pi/4$ are defined, the initial conditions become

$$\left.\begin{aligned} \eta_0 &= \tfrac{1}{4} J_0(\sigma), \\ u_0 &= 0, \\ x &= -\tfrac{\sigma^2}{16} + \tfrac{1}{4} J_0(\sigma), \end{aligned}\right\} \tag{43}$$

where σ is a new variable defined as $\sigma = 4\sqrt{-x + \eta_0}$. Besides, the seaward boundary is determined from exact solution. Given some x, the corresponding σ can be obtained with iteration by using Newton-Raphson method. Then, substituting σ into the first relation in (43) leads to the initial water elevation η_0. Figure 6 presents the comparison between the numerical results and their corresponding exact solutions. The wave runs down from $t = 3\pi/4$ and stops at $t = 5\pi/4$ with velocity $u = 0$ instantly. The comparison shows the scheme can closely approximate Carrier-Greenspan periodic solution.

4.3. Validation of the bottom-tilting wave maker

Given the bottom motion, the numerical method enables to approximate the evolution of the free surface waves, while the analytical solution gives a rough estimation. Cases in which the bottom moves at constant speed are considered for simplicity in the present study. Here, only upward or downward motion from the initial position θ_m is considered, where θ_m is the amplitude of the rotating angle. As shown in figure 2, rotating angle θ can be represented as $\theta(t) = \theta_m(1 - t/b)$, where b is the motion duration. Hence, the trajectory of the bottom for upward motion is described as

$$\begin{aligned} S(x,t) &= -h_0 - (L - x)\tan\theta \\ &\approx -h_0 - (L - x)(\theta_m - \theta_m/b \cdot t) \\ &\approx -h_0 - D_0(x)(1 - t/b), \end{aligned} \tag{44}$$

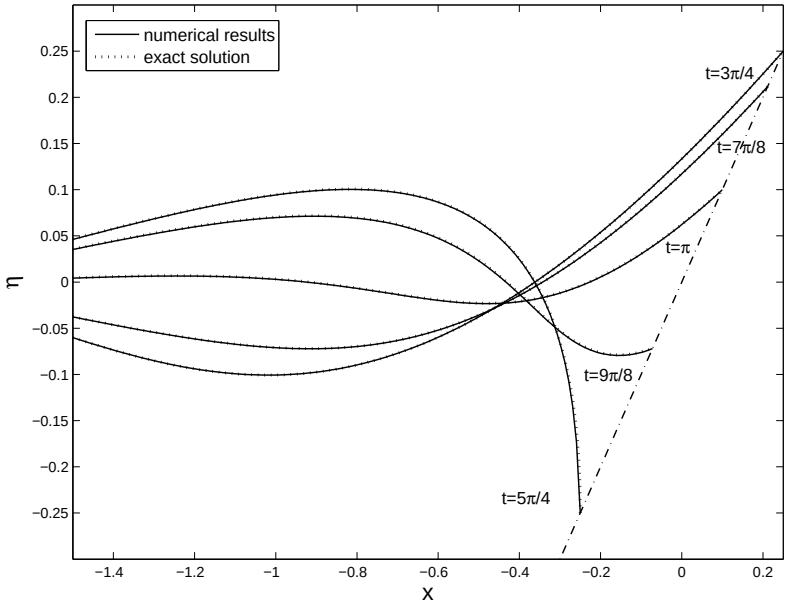

Figure 6: Comparison of the wave run-up model to Carrier-Greenspan periodic solution (solid line indicates the numerical results and dotted line indicates the exact solution).

Table 1: Parameters for varying bottom motions.

Parameters	Values
Water depth h_0 (m)	0.060, 0.050, 0.040,
Bottom motion displacement a (m)	0.005, 0.010 $\cdots$ 0.040
Bottom motion duration b (s)	0.5, 1.0, 1.5, 2.0

or for downward motion similarly:

$$S(x,t) \approx -h_0 + D_0(x)(1 - t/b), \tag{45}$$

where motion amplitude D_0 is already determined by (20). Thus, $B(t)$ is defined as

$$B(t) = \begin{cases} -(1 - t/b), & \text{upward motion,} \\ 1 - t/b, & \text{downward motion,} \end{cases} \tag{46}$$

so its time derivative $Q(t)$ is defined as

$$Q(t) = \begin{cases} 1/b, & \text{upward motion,} \\ -1/b, & \text{downward motion.} \end{cases} \tag{47}$$

Therefore, by substituting (47) into (24) for upward motion, the free surface elevation at the hinge becomes

$$\eta(L,t) = \begin{cases} \frac{aL}{\pi} \int_0^t du \int_0^\infty dk \, \frac{1}{b} \frac{\sin^2(kL/2)}{(kL/2)^2} \frac{\cos kL}{\cosh kh} \cos\omega(t-u), & 0 \le t \le b, \\ \frac{aL}{\pi} \int_0^b du \int_0^\infty dk \, \frac{1}{b} \frac{\sin^2(kL/2)}{(kL/2)^2} \frac{\cos kL}{\cosh kh} \cos\omega(t-u), & t \ge b. \end{cases} \tag{48}$$

Similarly, for downward motion, the bottom motion displacement leads to the free surface elevation at the hinge

$$\eta(L,t) = \begin{cases} -\frac{aL}{\pi} \int_0^t du \int_0^\infty dk \, \frac{1}{b} \frac{\sin^2(kL/2)}{(kL/2)^2} \frac{\cos kL}{\cosh kh} \cos\omega(t-u), & 0 \le t \le b, \\ -\frac{aL}{\pi} \int_0^b du \int_0^\infty dk \, \frac{1}{b} \frac{\sin^2(kL/2)}{(kL/2)^2} \frac{\cos kL}{\cosh kh} \cos\omega(t-u), & t \ge b. \end{cases} \tag{49}$$

Lu et al. (2016) carried out experiments and the parameters used for wave generation are summarized in table 1, in which the moving bottom length is $L = 1\,m$. Note that the following results are demonstrated in dimensionless form.

First of all, figure 7 shows the comparison of time history of the free surface elevation at hinge between experimental data and theoretical results, where (a) shows the waves generated by upward motion and (b) downward motion, with $h_0 = 0.05\,m$,

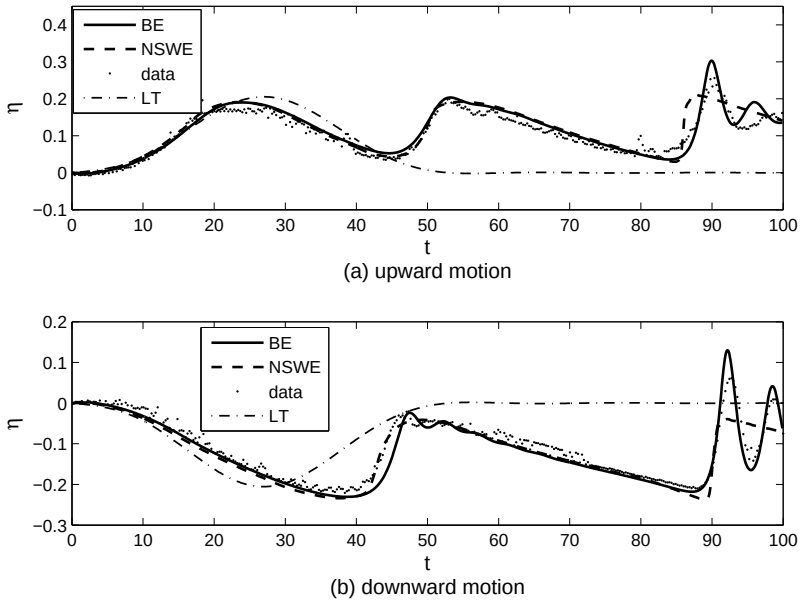

Figure 7: Comparison of free surface elevation at hinge (BE: Boussinesq equations, NSWE: nonlinear shallow water equations, LT: linear wave theory).

$a = 0.025\,m$ and $b = 1.0\,s$. Apparently, the numerical model based on Boussinesq equations can closely approximate the waves generated by the new wave maker. The numerical results by solving nonlinear shallow water equations show good agreement with the experimental data as well, but cannot simulate the dispersion in the generation region. Therefore, Boussinesq equations have better performance than nonlinear shallow water equations for wave generation, in particular the later period of time. Compared to the analytical solution by linear wave theory for the leading wave, the numerical results display a slight asymmetry, in particular the downward motion, which is caused by marked nonlinearity in this shallow water tank. Thus, nonlinear effects can not be ignored even for wave generation in this wave tank. Still, linear wave theory can be useful for quick estimate.

Wave amplitude and wave period of the resulting waves are the main features to be examined for wave generation. The influences of varying bottom motion displacement a and duration time b on the amplitudes and periods of the resulting leading waves are respectively shown in figure 8 for upward motion and figure 9 for downward motion with water depth of 0.05 m.

The figures confirm again that the Boussinesq equation system approximates the experimental data well. In particular, the analytical solution cannot predict the dependence of the wave period T on the bottom displacement a, which is a nonlinear effect.

Besides, by applying the run-up numerical model, the maximum run-up of different generated waves is compared to experimental data (Lu et al., 2016) and shown in figure 10 (a) for upward bottom motion and figure 10 (b) for down-upward bottom motion. Here, the varying bottom motion displacements a in dimensionless form are different from the wave generation investigation, which ranges from 0.17 to 0.67 now, since the water depth is limited within 0.03m to ensure run-up can be completely observed without touching the wall at the top of the slope in the experiments. Clearly, the numerical results can successfully model the experimental data by choosing appropriate drag coefficient.

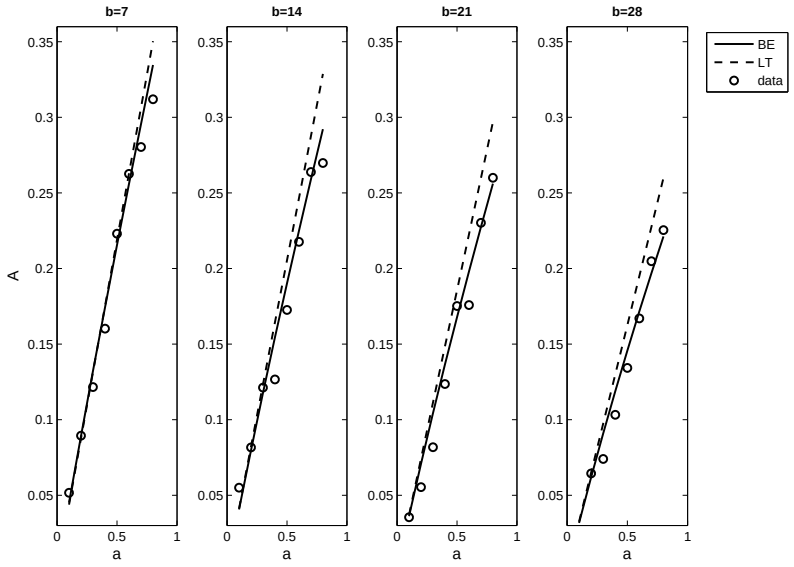

(a) Wave amplitude A with varying motion parameters a and b

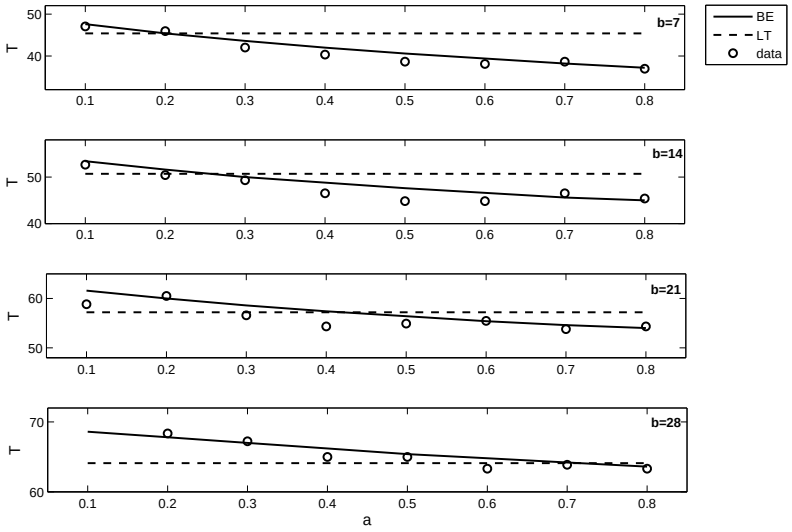

(b) Wave period T with varying motion parameters a and b

Figure 8: Relations between the bottom motion parameters (amplitude a and duration b) and the characteristics of the resulting wave (amplitude A and period T) for upward motion (dotted line, solid line and circle indicate results by linear wave theory, Boussinesq equations and measurements, respectively).

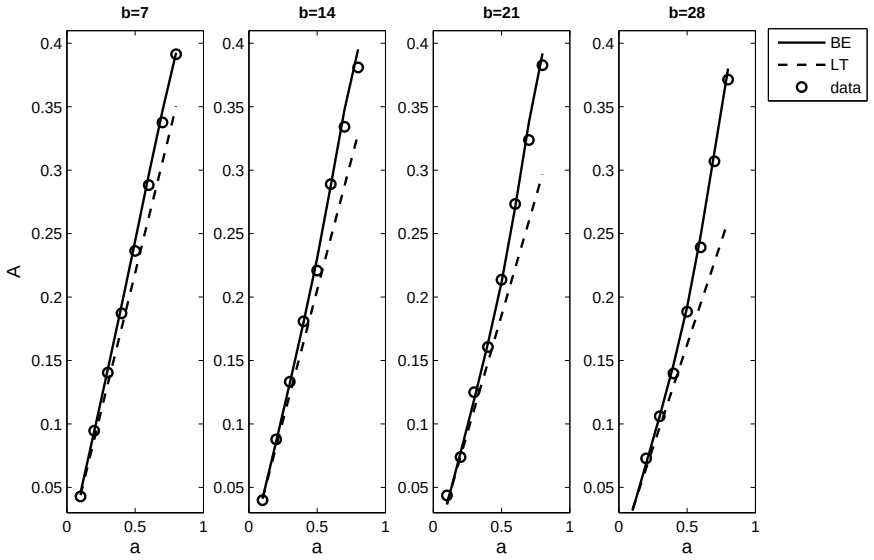

(a) Wave amplitude A with varying motion parameters a and b

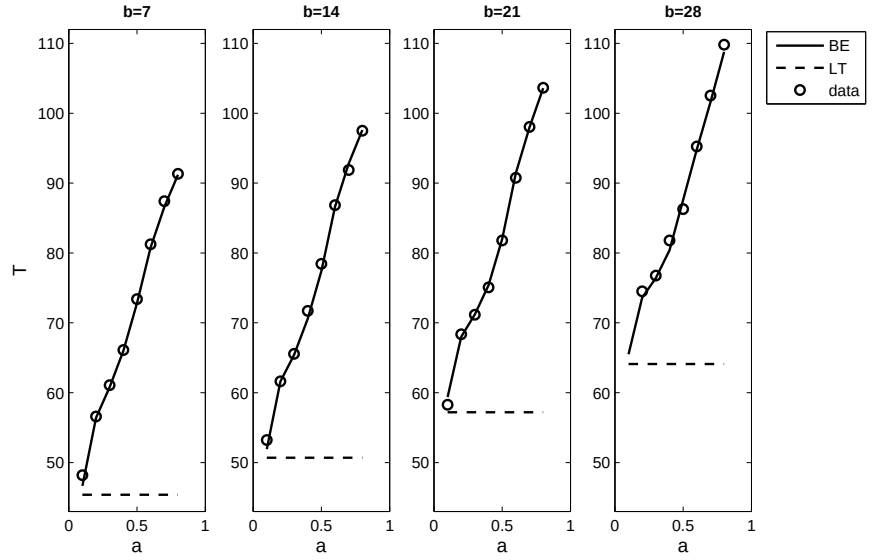

(b) Wave period T with varying motion parameters a and b

Figure 9: Relations between the bottom motion parameters (amplitude a and duration b) and the characteristics of the resulting wave (amplitude A and period T) for downward motion (dotted line, solid line and circle indicate results by linear wave theory, Boussinesq equations and measurements, respectively).

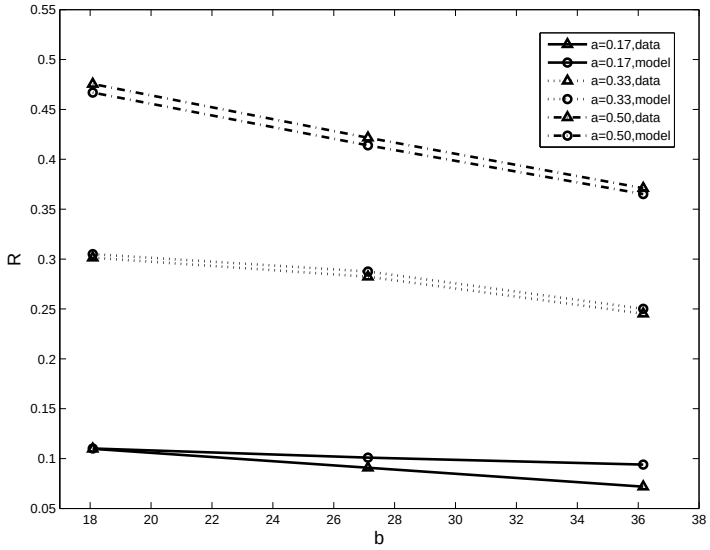

(a) Upward motion

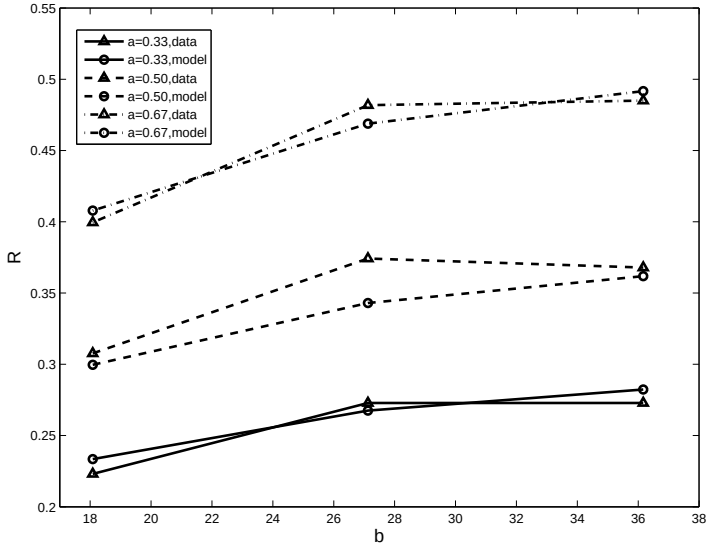

(b) Downward motion

Figure 10: Relations between the bottom motion parameters (motion amplitude a and motion duration b) and the maximum run-up R (triangle and circle indicate measurements and numerical results, respectively).

5. Conclusions

The new wave generator used in this study is a bottom-tilting wave maker, which makes very long waves by moving the bottom hinged at the toe of the beach with adjustable slope under the command of an electric servo motor. This new type of wave maker is built because of the query of whether solitary wave is able to represent the geophysical scales of tsunamis or not arisen by recent researches. In other words, it is of great importance to generate waves that are longer than solitary waves in laboratory.

Some theoretical methods are used and discussed for modelling this bottom-tilting wave maker. The linear wave theory can provide the estimation of the leading order of the waves generated. Furthermore, a numerical model based on the nonlinear shallow water equation has been built to approximate the evolution of the surface waves for more practical consideration. Additionally, another numerical model based on weakly nonlinear and weakly dispersive wave theory has been built for only wave generation. Finite volume discretization combined with reconstruction methods (UNO, WENO) has been used to numerically solve the equations, which is conservative and shock-capturing.

Numerical schemes have been verified by various validation tests. Then, good agreement between the theoretical results and the experimental measurements confirms that the numerical model can model the generated wave accurately, both in wave generation and wave run-up. Moreover, it should be noted that nonlinear effects are important and necessary to be taken into consideration for practically modelling the waves generated by this new wave maker. For wave generation, including dispersion in the numerical model is helpful in simulating higher order waves more accurately. Thus, surface waves studied in Boussinesq scaling with time-dependent bottom bathymetry gives a better performance in approximating the wave generation, while nonlinear shallow water system is good at approximating the wave run-up.

We remark here that active absorption of the reflected waves needs to be considered for this wave maker to be more practical. We have not discussed the issue here as the focus is on modelling of the waves during and immediately after the generation stage. Within the linear theory, it can be shown that active absorption is possible without

modification of the wave tank. We will further pursue this subject in the future work.

6. Acknowledgements

YSP acknowledges financial support from the Royal Society of Edinburgh through the Royal Society of Edinburgh and Scottish Government Personal Research Fellowship Co-Funded by the Marie-Curie Actions. This research is supported by the financial support from the Korea Institute of Marine Science and Technology Promotion [Reference No. 20140437].

Antuono, M. and Brocchini, M. 2007. The boundary value problem for the nonlinear shallow water equations. *Studies in Applied Mathematics*, 119(1):73–93.

Antuono, M. and Brocchini, M. 2010. Solving the nonlinear shallow-water equations in physical space. *Journal of Fluid Mechanics*, 643:207–232.

Antuono, M., Hogg, A. J., and Brocchini, M. 2009. The early stages of shallow flows in an inclined flume. *Journal of Fluid Mechanics*, 633:285–309.

Bogacki, P. and Shampine, L. 1989. A 3(2) pair of Runge-Kutta formulas. *Appl. Math. Lett.*, 2(4):321–325.

Carrier, G. F. and Greenspan, H. P. 1958. Water waves of finite amplitude on a sloping beach. *J. Fluid Mech.*, 4(01):97–109.

Craig, W. 2006. Surface water waves and tsunamis. *J. Dyn. Differ. Equ.*, 18(3):525–549.

Dutykh, D. and Kalisch, H. 2013. Boussinesq modeling of surface waves due to underwater landslides. *Nonlinear Proc. Geoph.*, 20(3):267–285.

Dutykh, D., Katsaounis, T., and Mitsotakis, D. 2011. Finite volume schemes for dispersive wave propagation and runup. *J. Comput. Phys.*, 230(8):3035–3061.

Goring, D. G. 1978. *Tsunamis–the propagation of long waves onto a shelf*. PhD thesis, California Institute of Technology.

Hammack, J. L. 1973. A note on tsunamis: their generation and propagation in an ocean of uniform depth. *J. Fluid Mech.*, 60(04):769–799.

Harten, A. and Osher, S. 1987. Uniformly high-order accurate nonoscillatory schemes. i. *SIAM J. Numer. Anal.*, 24(2):279–309.

Kajiura, K. 1963. The leading wave of a tsunami. *B. Earthq. Res. I. Tokyo*, 41:535–571.

Keller, J. B. and Keller, H. B. 1964. Water wave run-up on a beach. Technical report, U.S. Department of the Navy.

Kit, E., Shemer, L., and Miloh, T. 1987. Experimental and theoretical investigation of nonlinear sloshing waves in a rectangular channel. *Journal of Fluid Mechanics*, 181:265–291.

Li, Y. and Raichlen, F. 2002. Non-breaking and breaking solitary wave run-up. *J. Fluid Mech.*, 456:295–318.

Liu, D. and Lin, P. 2008. A numerical study of three-dimensional liquid sloshing in tanks. *Journal of Computational Physics*, 227(8):3921–3939.

Liu, P. L.-F., Cho, Y.-S., Briggs, M. J., Kanoglu, U., and Synolakis, C. E. 1995. Runup of solitary waves on a circular island. *J. Fluid Mech.*, 302:259–285.

Liu, X.-D., Osher, S., and Chan, T. 1994. Weighted essentially non-oscillatory schemes. *J. Comput. Phys.*, 115(1):200–212.

Lu, H., Park, Y.-S., and Cho, Y.-S. 2016. Parametric study of bottom-tilting wave maker. *In Preparation*.

Madsen, P. A., Fuhrman, D. R., and Schäffer, H. A. 2008. On the solitary wave paradigm for tsunamis. *J. Geophys. Res.*, 113(C12012).

Madsen, P. A. and Schäffer, H. A. 2010. Analytical solutions for tsunami runup on a plane beach: single waves, N-waves and transient waves. *J. Fluid Mech.*, 645:27–57.

Mei, C. C. 1989. *The Applied Dynamics of Ocean Surface Waves*, volume 1. World scientific.

Peregrine, D. H. 1967. Long waves on a beach. *J. Fluid Mech.*, 27(04):815–827.

Shu, C.-W. 1998. Essentially non-oscillatory and weighted essentially non-oscillatory schemes for hyperbolic conservation laws. In Quarteroni, A., editor, *Advanced Numerical Approximation of Nonlinear Hyperbolic Equations*, volume 1697 of *Lecture Notes in Mathematics*, pages 325–432. Springer Berlin Heidelberg.

Sweby, P. K. 1984. High resolution schemes using flux limiters for hyperbolic conservation laws. *SIAM J. Numer. Anal.*, 21(5):995–1011.

Synolakis, C. E. 1987. The runup of solitary waves. *J. Fluid Mech.*, 185:523–545.

Tuck, E. O. and Hwang, L.-S. 1972. Long wave generation on a sloping beach. *J. Fluid Mech.*, 51(03):449–461.

Tyvand, P. A. and Miloh, T. 2012. Incompressible impulsive sloshing. *Journal of Fluid Mechanics*, 708:279–302.

Wu, T. Y.-T. 1987. Generation of upstream advancing solitons by moving disturbances. *J. Fluid Mech.*, 184:75–99.

Zelt, J. 1991. The run-up of nonbreaking and breaking solitary waves. *Coastal Eng.*, 15(3):205–246.

Zhang, J. E. 1996. *Run-up of ocean waves on beaches*. California Institute of Technology.